Optical Force on Dielectric Nanorods Coupled to a High-Q Photonic Crystal Nanocavity

Y. C. Jian,*,† J. J. Xiao,*,‡ and J. P. Huang*,§

Department of Physics and Surface Physics Laboratory (National Key Laboratory), Fudan University, Shanghai 200433, China, Department of Electrical and Computer Engineering, Fitzpatrick Institute for Photonics and Department of Radiation Oncology, Duke University Medical Center, Durham, North Carolina 27708, Department of Physics and William Mong Institute of NanoScience and Technology, The Hong Kong University of Science and Technology, Clear Water Bay, Hong Kong, China, and Department of Electronic and Information Engineering, Shenzhen Graduate School, Harbin Institute of Technology, Shenzhen 518055, China

Received: April 20, 2009; Revised Manuscript Received: August 10, 2009

It is of particular importance to bridge nanophotonics and nanomechanics by utilizing near-field-induced gradient forces to manipulate dielectric objects. On the basis of the finite-difference time-domain method, we theoretically study nanocavity-resonator-induced optical forces on different dielectric nanorods. The optical system consists of a nanorod which is optically coupled to a photonic crystal slab with a predesigned L3 nanocavity that has a resonant mode of high-quality factor $Q \approx 10^4$ and small modal volume 0.1 μm^3. Tunable attractive and repulsive (bipolar) optical forces on the nanorod are discovered, which crucially depend on the size of the nanorod and its separation from the slab. The magnitude of the force is revealed to be on the order of 10^3 pN with source irradiance $I = 10$ mW/μm^2 for a nanorod of size around $200 \times 100 \times 100$ nm^3 at a separation $d = 100$ nm. The results are compared with those by the Rayleigh scattering approximation, which suggests that the optical force is dominated by the gradient force due to the strong local field around the nanocavity. We further demonstrate the optomechanical stability of the system. Such a system provides a promising integrated on-chip platform for all-optical operation of nanomechanical devices.

Downloaded by IMPERIAL COLL LONDON on September 24, 2009 | http://pubs.acs.org
Publication Date (Web): September 3, 2009 | doi: 10.1021/jp903617a

I. Introduction

It has been a lengthy pursuit to harness a weak light force to maneuver tiny nanomachines and to utilize the pushing effect from solar photons, which can possibly provide necessary driving energy during interplanetary travel. Over the past decades, many simulations and experiments show the great potential of such bridges between nanophotonics and nanomechanics, by using concentrated light to manipulate semiconductor or biological objects in nanoscale, at high precision and accuracy.[1−7] Recently, a tunable optical force is experimentally achieved in several optomechanical systems,[8−11] while current on-chip exploitation of the optical force still lacks a highly localized light source, which can enable near-field optical manipulations operating under different circumstances.

The idea that nanocavities of photonic crystal slabs (PCSs) can provide an optical trap effect is preceded by an optical tweezer, which is regarded as a cornerstone in atomic and condensed matter physics and in biology instruments. Optical tweezers were first proposed by Ashkin and later greatly developed in biology,[6,7] using the concentrated gradient potential nature of a tightly focused laser beam to trap small particles, virus, or bacterium cells ranging in size from several micrometers to a few hundred nanometers. However, the manipulation of objects with smaller size demands much stronger confinement of light beyond the normal diffraction limit. Due to the ease of design and fabrication, PCS nanocavities are a promising candidate for the next generation of near-field optical tweezing, as they provide a highly compacted and easily "accessible" optical mode in nanoscale.[12−19] The strongly confined electromagnetic field inside the cavity leads to an enhanced light−matter interaction, which gives the possibility of ultrasmall laser, optical switching, chemical sensing, and nanoparticle micromanipulation. Such cavities can also be applied in fluidic systems,[20] where the fluid fills the cavity or flows in the vicinity of the cavity, thereby modifying the refractive index; rather rigorous considerations for such a system include complex drag forces and velocity effects.[21]

The first near-field optical potential distribution in a PCS cavity was reported in 2006 by Rahmani et al.[12] Calculations have shown that, for such structures, the electromagnetic field is tightly confined within a specific region, which could lead to a strong optical gradient force on small particles. However, the way to manipulate dielectric objects using the near-field-induced gradient force still remains largely unexplored. In this article, we consider such a PCS nanocavity with a very high resonant quality factor (up to $Q \approx 10^4$), where the mutual optical interaction between the cavity's resonant mode and the dielectric particle is no longer negligible. The presence of the particle affects the optical resonant mode and therefore the gradient potential in the vicinity of the PCS, which would pull or push the particle to a possible equilibrium position. Through evanescent wave (near field) coupling, there is a strong optical interaction and momentum exchange between the nanoparticle and the PCS nanocavity. It is worth mentioning that such a cavity-enhanced optical force was observed in a microdisk coupled to a waveguide ring, showing an extraordinary optomechanical effect.[3] As also shown by Koenderink et al. in numerical simulations,[13] the insertion of a dielectric-tip probe slightly tunes the eigen-frequency of an ultrahigh-Q nanocavity and reduces its quality factor. Our simulations will show that,

* To whom correspondence should be addressed. E-mails: yuchuan.jian@duke.edu; jjxiao@ust.hk;jphuang@fudan.edu.cn.
† Fudan University and Duke University.
‡ Hong Kong University of Science and Technology and Harbin Institute of Technology.
§ Fudan University.

10.1021/jp903617a CCC: $40.75 © 2009 American Chemical Society
Published on Web 09/03/2009

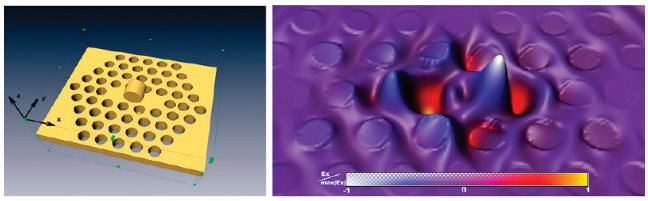

(a) (b)

Figure 1. (a) Schematic graph showing the system of a nanorod coupled with the cavity of a PCS. Notice the system axis z is perpendicular to the slab (xy plane) in the figure. (b) The profile of electric field component E_x of the fundamental L3 cavity mode. The electrical field is normalized by the maximum value of E_x.

in the presence of nanoparticles, a resonant-frequency shift less than 1.4% is introduced into the cavity mode and the highest quality factor change is around 9% (without considering lateral radiation loss).

II. Model

The system under consideration consists of a nanorod made of a high-refractive-index material (e.g., conjugated polymer with dielectric constant $\varepsilon = 25$) on top of a PCS with the separation distance below 140 nm, as shown in Figure 1a. In all the calculations, the nanorod height (dimension along the y-axis) is kept at 200 nm and the radius of its cross section varies from 60 to 100 nm. A cavity (L3 cavity) is designed in the PCS ($\varepsilon = 11.56$, thickness $t = 180$ nm) with three consecutive air holes of radius $r = 60$ nm at the center of a periodic hexagonal lattice (lattice constant $a = 200$ nm) filled up (absence). Song et al. first showed that an ultrahigh-quality factor Q in such a PCS L3 cavity can easily be obtained by shifting the neighboring two air holes on the cavity edges to achieve a smooth electric field distribution, greatly reducing the vertical radiation loss.[16] Photons are then strongly confined in the PCS cavity for all the propagation directions, when the Bragg reflection conditions are achieved in the lateral directions. Since then, the L3 (and likewise) cavity aroused great interest in improving the Q-factor of a cavity in PCS and the structure is now utilized in picosecond light pulse application[17] and in cavity quantum electrodynamics of semiconductor quantum dots that couples to such PCS cavities.[18,19] L3 cavity structure is now still one of the best options for obtaining ultrahigh Q for certain resonances and can be easily fabricated and have been widely adopted over many nanodevices.[21] Many exotic phenomena—like vacuum Rabi splitting, reflectivity, and transparency—have been observed in such PCS cavities.[22] In our case, the cavity's end-edge hole shifting distance is 40 nm (see Figure 1a) and the simulated cavity optical mode (see the mode pattern in Figure 1b) has a resonant frequency $\omega a/2\pi c = 0.246$ (wavelength $\lambda = 813$ nm), quality factor $Q \approx 10^4$ with modal volume $V = 0.1\ \mu\text{m}^3$ (smaller than the fundamental limit $(\lambda/2n)^3$). The correspondent line width is $\Delta\lambda \approx 0.12$ nm. The dielectric nanorod is optically coupled to this resonant mode, which is excited by an external source at the resonant frequency.

The finite-difference time-domain (FDTD) technique[23,24] is applied to calculate the distribution of the Poynting vector and then to obtain the optical radiation pressure on the nanorod, which can be decomposed into the scattering and gradient forces. The FDTD technique divides space and time into rectangular Yee grid, discretizing Maxwell's equations with first-order accuracy.[23,24] Standard perfectly matched layers (PMLs) are used at the computational boundaries, providing absorbing boundary condition in the z direction. We use the FDTD-based Maxwell's stress tensor algorithm for the force calculation and analysis.[25] According to the conservation of momentum, Maxwell's stress tensor σ_{ik} of an object with volume V and surface area A in an electromagnetic field satisfies the relationship[26,27]

$$\frac{\partial}{\partial t}\int P_i\,\mathrm{d}V + \frac{\partial P_{0i}}{\partial t} = -\int \sigma_{ik} n_k\,\mathrm{d}A \qquad (1)$$

where P_i represents the coordinate component of the total electromagnetic field's Poynting vector and n_k the normal unit component. Note that the optical mechanical force comes from the variation of the object's Poynting vector $\partial P_{0i}/\partial t$. The rigorous stress tensor on the object reads

$$\sigma_{ik} = \frac{\delta_{ik}}{2}(\varepsilon_0\varepsilon|E|^2 + \mu\mu_0|H|^2) - \varepsilon_0\varepsilon E_i E_k - \mu\mu_0 H_i H_k \qquad (2)$$

where ε and μ are the medium's permittivity and permeability, respectively. Similar to 2D objects like nanowires and nanotubes, which extend uniformly (translational invariant) in one direction, the optical force for the nanorod is $F_i = \mathrm{d}\bar{P}_{0i}/\mathrm{d}t = \int \bar{\sigma}_{ik} n_k\,\mathrm{d}A = \Delta\bar{S}_i L_x L_y/c$, which can be compared to the Rayleigh approximation.[28] The relationship is valid when the surrounding medium is air. The differential Poynting vector $\Delta\bar{S}$ is obtained by comparing the components of the electromagnetic vectors inside and outside the nanorod over several time cycles along (**E**, **H**) grid points in the region of interest,[29] thereby representing the change of the electromagnetic energy flow. From Figure 1a, we expect that the energy flow in the PCS plane (xy plane) is conserved. Also, it should be symmetric along the axis of the nanorod along the y direction and will not contribute to the optical force components. Therefore, it is much easier to obtain the optical force when the nanorod is elongated. In such cases, by virtue of symmetry in the system configuration, forces in the $+x$ and $-x$ and $+y$ and $-y$ directions cancel each other out; only the force along the z direction remains finite. The geometry of the system and arrangement of he nanorod ensures that there is only vertical (i.e., z-axis) force exerted on the nanorod.

III. Numerical Results

Figure 2 shows the typical Poynting vector strength in the nanorod−nanocavity system. The Poynting vector fields represent the energy flow in the system and indicate the radiation pressure on the nano-objects. For the drawing consideration of symmetry, we added another nanorod in $-z$ direction. Then, the Poynting vector of the system is symmetric in all the directions.

Figure 3 shows the averaged force density distribution in the plane of the nanorod's cross section (xz plane). The detailed geometry and other parameters can be found in the figure caption. The sharp ridges of some regions in the figure illustrate the force density of these areas is higher, and the profile lines below the center plane shows repulsive force. As for nanorods at two different separations, the side profiles of the optical force are symmetrical with respect to the x axis and asymmetrical about the z axis, which results from the mode profile (see Figure 1b) of the resonant mode in the PCS cavity and gives a net force in the z direction.

Figure 4 shows the distribution of the optical potential in the 3D space when the optical frequency of the nanocavity is fixed

Downloaded by IMPERIAL COLL LONDON on September 24, 2009 | http://pubs.acs.org
Publication Date (Web): September 3, 2009 | doi: 10.1021/jp903617a

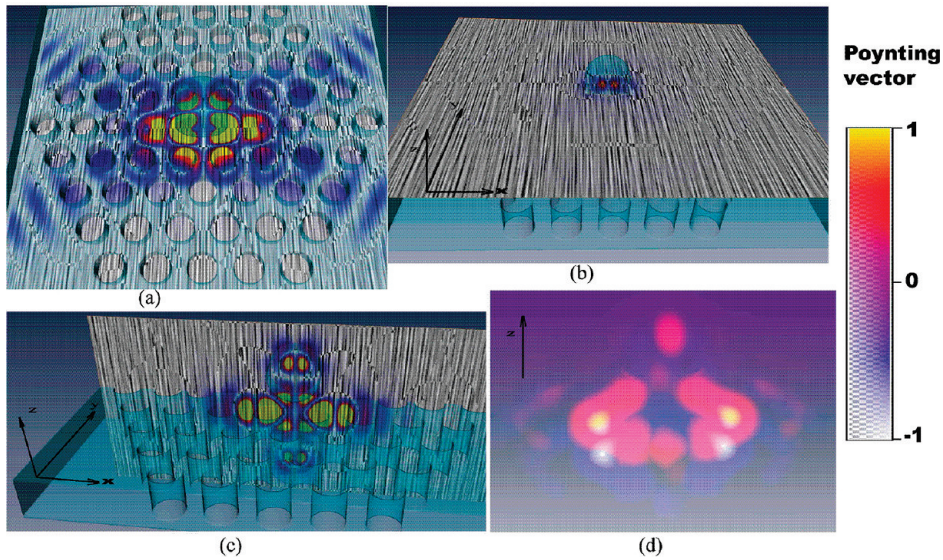

Figure 2. Three-dimensional distribution of the normalized Poynting vector in the coupled nanorod and PCS system, which represents the energy flux when photons are injected into the cavity. The grayish surface in (a−c) is to visualize vector field for its directional structure in one cutting plane using line integral convolution algorithm. (a) Projection of the Poynting vector on the cross-sectional plane of the PCS (*xy* plane) using a line integral convolution algorithm.[29] (b) Projection of the Poynting vector on the cross-section of the nanorod (*xy* plane). (c) The Poynting vector's projection on the cross section of the PCS (*xz* plane). (d) The volume rendered Poynting vector distribution.

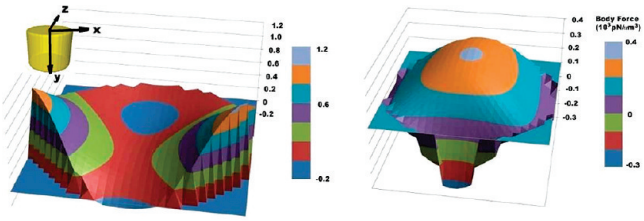

Figure 3. The side profile of the optical force per unit volume, distributed on the nanorod's cross section (*xz* plane). The irradiation source power is 10 mW/μm^2 in the nanocavity region. (a) The geometrical parameters are nanorod radius $r = 100$ nm and the separation distance from the PCS surface $d = 20$ nm; (b) the geometry is changed to $r = 80$ nm and $d = 10$ nm. The positive value of force shows the attractive exertion on the nanorod toward the slab, and vice versa.

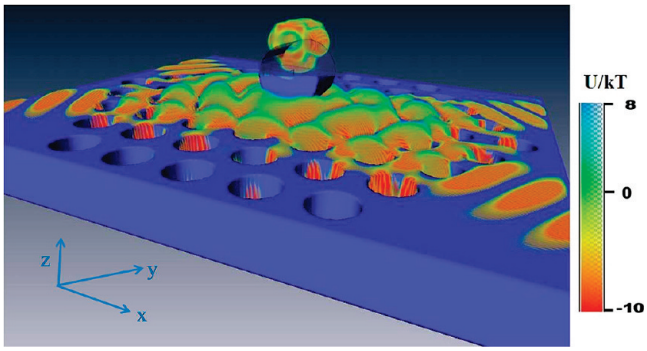

Figure 4. Distribution of the normalized electromagnetic energy in the coupled system. An attractive optically induced potential ball is formed in the top part of the nanorod. Here, k is the Boltzmann constant and T the room temperature.

at 369 THz (wavelength 810 nm), which is ideal for high-speed MEMS operation of mechanical resonance oscillation.[30] The results in this figure are for the case in which the radius of the nanorod is $r = 100$ nm and the nanorod−cavity separation is increased from $d \leq 20$ nm (as in Figure 3) to $d = 130$ nm. The magnitude of the optical potential is normalized to the maximum absolute value. Note that the repulsive potential (light blue in color) dominates in the area between the bottom of the nanorod

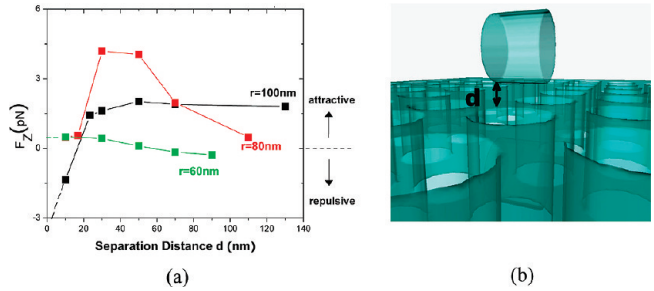

Figure 5. (a) Optical force as a function of the distance d between the nanorod and the PCS, as schematically shown in (b). The error bar is not shown on the diagram, and it is within 5% of the value displayed. The main error comes from the grid point selection for the force distribution in the vicinity of the nanorod after the FDTD simulations.

and the surface of the PCS. On the top z-section of the nanorod, there is an energy ball that provides most heavy trapping potential (red in color) in the system. The position of trapping ball also manifests the asymmetric distribution of optical force along the z-direction as shown in Figure 3. For nanorods of different locations and/or sizes, the balanced optical potential is different and determines whether the attractive or repulsive optical force emerges. As the separation between the nanorod and PCS decreases, larger area of repulsive potential is observed. We also notice that the air holes of the PCS always have attractive potential when the separation distance and nanorod size change.

The detailed calculations for the separation and size-dependent forces are shown in Figure 5a. For clearance, the separation in the coupled system is as defined in Figure 5b. If the separation is reduced to $d = 10$ nm, the nanorod ($r = 100$ nm) will experience a strongly repulsive force (for convention, a positive sign stands for an attractive force since the $-z$ direction toward the PCS as depicted in Figure 1a). Further calculations show that, when the nanorod is closer to the slab surface, the optical mode of the PCS cavity will be deteriorated, this is as expected according to the relationship[31] $1/Q_{tot} = 1/Q_{cavity} + 1/Q_{coup}$, where Q_{cavity} is the quality factor of the isolated nanocavity and Q_{coup}

Downloaded by IMPERIAL COLL LONDON on September 24, 2009 | http://pubs.acs.org
Publication Date (Web): September 3, 2009 | doi: 10.1021/jp903617a

Downloaded by IMPERIAL COLL LONDON on September 24, 2009 | http://pubs.acs.org
Publication Date (Web): September 3, 2009 | doi: 10.1021/jp903617a

the optical coupling, which increases dramatically as the nanorod approaches the PCS cavity (i.e., as d decreases). Thus, by exploiting the optical force characteristics, a nanorod with a large radius $r \geq 100$ nm can be trapped so that it floats on top of the PCS considering its gravity which is an order of magnitude smaller than the optical force. For further increased separation, the nanorod does not disturb the optical mode much and the force becomes attractive. The force will eventually go to zero when the separation distance is large enough. However, for a smaller nanorod with radius $r \leq 60$ nm (notice that the air hole has radius of 60 nm), the force characteristics are quite reversed (see Figure 5a): when it approaches the PCS cavity, there is an increased attractive force and the nanorod will eventually enter the air holes of the PCS. It is then expected that the resonant cavity mode would be influenced dramatically; however, the mode could still survive. For such nanorods, polymer dispersed materials like fluidic liquid crystals can be used to seal the air holes to prevent them from disturbing the optical mode,[32,33] which would slightly change the refractive index of the PCS. Finally, the optical cavity mode is found to be completely degraded when nanorods with an intermediate radius between 60 and 100 nm approach the PCS cavity well below $d = 30$ nm. For example, as seen in Figure 5a, the force curve for the case of $r = 80$ nm drops quickly to zero as the nanorod is either too far or too close to the PCS. Applications using the observed bipolar force features for differently sized nanorods are numerous, such as cell/DNA isolation, molecule sieving,[34] and local sample preconcentration.[35] We note that the mechanism for bipolar optical forces here is different from that for whispering-gallery mode induced ones in dielectric particles, which are excited by an evanescent wave.[31]

With a bipolar optical force observed, we go one step further to analyze the origin of such attractive and repulsive forces from another perspective: if we treat the nanorod as a dielectric waveguide, its effective index will also change when the photon frequency shifts. Even though the operating wavelength is much longer than the size of the nanorod, the resonant mode of the cavity can result in a heavily modulated field near the nanorod. The closed optical system has the following dispersive relationship[36] $(\Delta\omega)/(\omega) = (\Delta\lambda)/(\lambda) = -(\Delta n)/(n_g)$, where Δn is the effective index change and $n_g = c[(\partial k)/(\partial\omega)]$ is the group index of the waveguide. It is well-known that the separation distance can possibly induce a sign change of the effective index in the waveguide.[3] Therefore, both negative and positive forces can be obtained with different guided modes.

As mentioned above, the optical force exerted on the nanorod is similar to that from the Rayleigh scattering approximation, which is valid when the particles are much smaller than the light's wavelength such that its optical response can be regarded as a simple dipole. For our case, the average length scale of the nanorods is about 100 nm, which is much smaller than the wavelength of light used here (more than 800 nm), so we can invoke the Rayleigh approximation to better understand our results. In the Rayleigh limit, the gradient force is given by $F_{scat} = [(\alpha)/(2)]\nabla|E|^2$, where α is the polarizability factor of the nanoparticle.[37] For a particle with cylindrical-like structure, the polarizability factor of the gradient force is[38,39]

$$\alpha = \frac{2}{3}\pi\varepsilon_0 V\left(\frac{n^2 - 1}{1 + N(n^2 - 2)}\right) \approx 2\pi(n - 1)\varepsilon_0 V = 2\pi\Delta n\varepsilon_0 V \quad (3)$$

Plugging the specific dielectric constant of nanorod into the above equation, we have $\alpha \approx \varepsilon V$. Here, N is the depolarization factor, n the refractive index of the nanorod, and V the volume of the nanorod. Figure 6 shows the optical gradient force distribution when the nanorod approaches the PCS. The yellow arrows in the figure show in detail the complex gradient force behavior around the air holes of L3 structure in the PCS. It is shown that optical energy with the strongest gradient is in the area of nanocavity and the air holes.

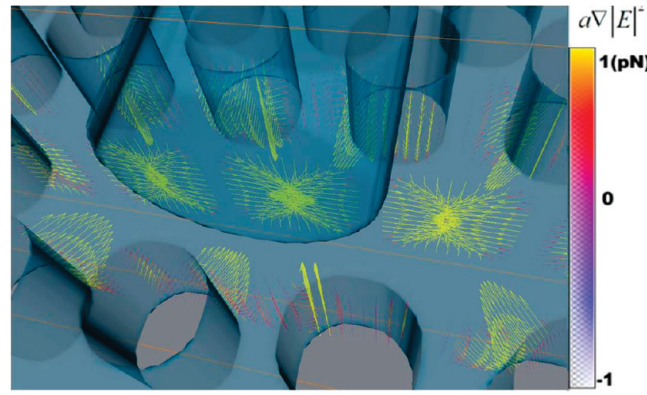

Figure 6. The magnitude and direction of the gradient force around and inside the PCS. The components of $\alpha\nabla|E|^2$ are projected on the xz plane. Parameters: PCS thickness, 180 nm; air hole diameter, 60 nm; nanorod radius, 80 nm; and distance from the PCS surface, 20 nm.

Finally, we evaluate the stability of the coupled nanorod−cavity system. In order to analyze this system, we calculate the force required to move the nanorod that sits at a particular position. First, we assume that the nanorod floats on the top of the slab in the equilibrium state and we treat the whole system as a closed one. Then, the nanorod is perturbed downward by a small distance Δd, which is regarded as an adiabatic process: both the absorption mechanisms in the constituent materials of the PCS and the radiation loss are ignored. During this process, the optical frequency of the cavity will simultaneously be changed by $\Delta\omega$ if a particular mode is present. The electromagnetic energy U is the dominant factor inducing the mechanical force because the energy conservation condition results in the required force on the nanorod[39]

$$F = -\frac{\Delta U}{\Delta d} = -\frac{U}{\omega}\frac{\Delta\omega}{\Delta d} \quad (4)$$

We use the quantum nature of photons in the derivation process of the equations. The initial energy of the closed system is from the injected photons into the PCS cavity and can be estimated as $U = N_p\hbar\omega$, where $\hbar$ is the reduced Planck constant, N_p the total number of photons which are initially in the nanocavity, and $\hbar\omega$ is the energy per photon. Figure 7 shows the results of the nanorod's shifting force. The scale of the shifting force is in the order of $\sim\mu$N, which is far greater than typical optical force (in the order of pN). The stability of the coupled system is thus revealed. The nonlinear relationship between the optical force and spatial displacement shows the opt-mechanical effect due to the exceptional cavity figure of merit (Q/V), which would give rise to an asymmetric transmission spectrum when the light penetrates the nanorods.

The energy conversion efficiency of the mechanical control over the nanorod is another factor of our interest, which is also an important issue for the optomechanical coupling. The location of the nanorod can be controlled and manipulated by slightly adjusting the optical frequency of the nanocavity, such as in resonance Raman process and deformable Fabry−Perot optical

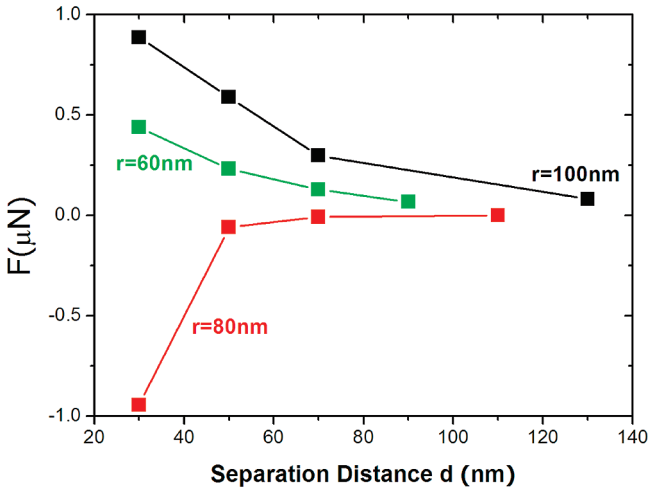

Figure 7. Optical forces F required to make the nanorod lower from the PCS surface, for three sizes of the cross section of nanorods: $r =$ 100 nm, $r = 80$ nm, and $r = 60$ nm.

cavity.[41] The energy efficiency in our system is determined by the high electromagnetic coupling mechanism between the nanocavity and the nanorod. So, increasing the absorption and transmission of photons in the nano-object by evanescent wave coupling is a good method to enhance the total energy conversion.

IV. Discussion and Conclusion

We have reported the possibility of using nanocavities of PCSs (photonic crystal slabs) in manipulating, sorting, and selecting dielectric nanoparticles. The force on the nanoparticles mainly originates from the cavity-enhanced optical dipole force, due to a Fabry−Perot-like resonance in the nanocavity. The system demonstrates a tunable and reconfigurable all-optical coupling. Our optomechanical device can also be used as low-power monitoring and sensing device such as chemical detector, which can maintain its functionality with high robustness. It can further be used to mechanically control the miniaturized optical elements which are frozen in the circuits. We have also carried out a detailed analysis on the relationship between the optical force and the size of the nanoparticle, and justified the equilibrium and stability of the system.

In summary, we have studied a coupled nanorod−nanocavity system and found tunable, bipolar optical forces. Such interactions form the foundation for the operation of a new class of light force devices and circuits. The use of a high-Q nanocavity resonance as a near-field optical maneuvering tool is beneficial. The optical cavity could enhance the robustness and reconfigurability of an opto-mechanical system, enabling spatial control of optical force over a flexible geometrical structure. The adaptive nanocavity resonator also introduces an important relationship between the localized photon energy and the system configuration, which stabilizes a nanoparticle and can be used to monitor nanophotonic components. Future extensions of this work could be on different kinds of nanorods, such as metallic or gradient nanowires, nanotubes, and doped nanoparticles,[40−45] in an attempt to enhance the coupling efficiency through intensifying the evanescent field strength and coupling efficiency. The sensitive optical force response to the geometric structure in the strongly coupled system indicates that the nanocavity has the ability to adapt to the environment in a complex nanoelectromechanical system.

Acknowledgment. This work has been supported by Chinese National Key Basic Research Special Fund under Grant No. 2006CB921706 and by the National Natural Science Foundation of China under Grant Nos. 10604014 and 10874025. YCJ would like to thank Dr. T. Yoshie for providing computation resources and Samuel Drezdzon for the help with the manuscript. Also, YCJ thanks Duke Scientific Visualization Program and Prof. Rachael Brady's fruitful help in data visualization.

References and Notes

(1) Grier, D. G. *Nature* **2003**, *424*, 810–816.
(2) Neuman, K. C.; Block, S. M. *Rev. Sci. Instrum.* **2004**, *75*, 2787–2809.
(3) Rakich, P. T.; Popović, M. A.; Soljaćić, M.; Ippen, E. P. *Nat. Photonics* **2007**, *1*, 658–665.
(4) Ashkin, A. *Phys. Rev. Lett.* **1970**, *24*, 156–159.
(5) Wineland, D. J.; Drullinger, R. E.; Walls, F. L. *Phys. Rev. Lett.* **1978**, *40*, 1639–1642.
(6) Ashkin, A.; Dziedzic, J. M.; Bjorkholm, J. E.; Chu, S. *Opt. Lett.* **1986**, *11*, 288–290.
(7) Ashkin, A.; Dziedzic, J. M. *Science* **1987**, *235*, 1517–1520.
(8) Li, M.; Pernice, W.; Xiong, C.; Baehr-Jones, T.; Hochberg, M.; Tang, H. *Nature* **2008**, *456*, 480–485.
(9) Li, M.; Pernice, W.; Tang, H. *Nat. Photonics* **2009**, *3*, 464–468.
(10) Eichenfield, M.; Jasper Chan, R. C.; Vahala, K. J.; Painter, O. *Nature* **2009**, *459*, 550–555.
(11) Unterreithmeier, Q. P.; Weig, E. M; Kotthaus, J. P. *Nature* **2009**, *458*, 1001–1004.
(12) Rahmani, A.; Chaumet, P. C. *Opt. Express* **2006**, *14*, 6353–6358.
(13) Koenderink, A. F.; Kafesaki, M.; Buchler, B. C.; Sandoghdar, V. *Phys. Rev. Lett.* **2005**, *95*, 153904.
(14) Akahane, Y.; Asano, T.; Song, B.-S.; Noda, S. *Nature* **2003**, *425*, 944–947.
(15) Loncar, M.; Hochberg, M.; Scherer, A.; Qiu, Y. *Opt. Lett.* **2004**, *29*, 721–723.
(16) Song, B. S.; Noda, S.; Asano, T.; Akahane, Y. *Nat. Mater.* **2005**, *4*, 207–210.
(17) Asano, T.; Kunishi, W.; Song, B.-S.; Noda, S. *Appl. Phys. Lett.* **2006**, *88*, 151102.
(18) Yoshie, T.; Scherer, A.; Hendrickson, J.; Khitrova, G.; Gibbs, H. M.; Rupper, G.; Ell, C.; Shchekin, O. B.; Deppe, D. G. *Nature* **2004**, *432*, 200–203.
(19) Englund, D.; Faraon, A.; Fushman, I.; Stoltz, N.; Petroff, P.; Vuckovic, J. *Nature* **2007**, *450*, 857–861.
(20) Schmidt, B. S.; Yang, A. H.; Erickson, D.; Lipson, M. *Opt. Express* **2007**, *15*, 14322–14334.
(21) Kuramochi, E.; Notomi, M.; Mitsugi, S.; Shinya, A.; Tanabe, T. *Appl. Phys. Lett.* **2006**, *88*, 041112.
(22) Faraon, A.; Fushman, I.; Englund, D.; Stoltz, N.; Petroff, P.; Vuckovic, J. *Opt. Express* **2008**, *16*, 12154–12162.
(23) Yee, K. S. *IEEE Trans. Antennas Propagation* **1966**, *14*, 302–307.
(24) Taflove, A.; Hagness, S. C. *Computational Electrodynamics: The Finite-Difference Time-Domain Method*; Artech House Publishers: Boston, 2005.
(25) Gauthier, R. *Opt. Express* **2005**, *13*, 3707–3718.
(26) Landau, L. D.; Lifshitz, E. M. *Mechanics and Electrodynamics*; Pergamon: Oxford, 1972.
(27) Kotlyar, V. V.; Nalimov, A. G. *Opt. Express* **2006**, *14*, 6316–6312.
(28) Ng, L. N.; Luff, B. J.; Zervas, M. N.; Wilkinson, J. S. *J. Lightwave Technol.* **2000**, *18*, 388–400.
(29) Cabral, B.; Leedom, L. C. Proceedings of the 20th annual conference on Computer graphics and interactive techniques. *ACM SIGGRAPH* **1993**, 263–270.
(30) Notomi, M.; Taniyama, H.; Mitsugi, S.; Kuramochi, E. *Phys. Rev. Lett.* **2006**, *97*, 023903.
(31) Xiao, J. J.; Ng, J.; Lin, Z. F.; Chan, C. T. *Appl. Phys. Lett.* **2009**, *94*, 011102.
(32) van der Heijden, R.; Carlström, C. F.; Snijders, J. A. P.; van der Heijden, R. W.; Karouta, F.; Nötzel, R.; Salemink, H. W. M.; Kjellander, B. K. C.; Bastiaansen, C. W. M.; Broer, D. J.; van der Drift, E. *Appl. Phys. Lett.* **2006**, *88*, 161112.
(33) Chou, C. F.; Bakajin, O.; Turner, S. W. P.; Duke, T. A. J.; Chan, S. S.; Cox, E. C.; Craighead, H. G.; Austin, R. H. *Proc. Natl. Acad. Sci. U.S.A.* **1999**, *96*, 13762–13765.
(34) Chou, C. F.; Zenhausern, F. *IEEE Eng. Med. Biol.* **2003**, *22*, 62–67.
(35) Svoboda, K.; Block, S. M. *Annu. Rev. Biophys. Biomol. Struct.* **1994**, *23*, 247–285.
(36) Rakich, P. T.; Popovic, M. A.; Watts, M. R.; Barwicz, T.; Smith, H. I.; Ippen, E. P. *Opt. Lett.* **2006**, *31*, 1241–1243.
(37) Venermo, J.; Sihvola, A. *J. Electrostat.* **2005**, *63*, 101–117.

Downloaded by IMPERIAL COLL LONDON on September 24, 2009 | http://pubs.acs.org
Publication Date (Web): September 3, 2009 | doi: 10.1021/jp903617a

(38) Gao, Y.; Jian, Y. C.; Zhang, L. F.; Huang, J. P. *J. Phys. Chem. C* **2007**, *111*, 10785–10791.

(39) Povinelli, M.; Johnson, S.; Lonèar, M.; Ibanescu, M.; Smythe, E.; Capasso, F.; Joannopoulos, J. *Opt. Express* **2005**, *13*, 8286–8295.

(40) Huang, J. P.; Yu, K. W. *Phys. Rep.* **2006**, *431*, 87–172.

(41) Favero, I.; Karrai, K. *Nat. Photonics* **2009**, *3*, 201–205.

(42) Maragò, O. M.; Jones, P. H.; Bonaccorso, F.; Scardaci, V.; Gucciardi, P. G.; Rozhin, A. G.; Ferrari, A. C. *Nano Lett.* **2008**, *8*, 3211–3216.

(43) Tan, S.; Lopez, H. A.; Cai, C. W.; Zhang, Y. *Nano Lett.* **2004**, *4*, 1415–1419.

(44) Simpson, G. J.; Wohland, T.; Zare, R. N. *Nano Lett.* **2002**, *2*, 207–210.

(45) Morandi, V.; Marabelli, F.; Amendola, V.; Meneghetti, M.; Comoretto, D. *J. Phys. Chem. C* **2008**, *112*, 6293–6298.

JP903617A

Downloaded by IMPERIAL COLL LONDON on September 24, 2009 | http://pubs.acs.org
Publication Date (Web): September 3, 2009 | doi: 10.1021/jp903617a